DTU Wind Energy

Modification of airfoil characteristics due to the influence of the free vortices in the wake of a rotor

Department of Wind Energy Master Report

Kaya Onur Dag

DTU Wind Energy Master Thesis M-0026

September 2013

DTU Vindenergi
Institut for Vindenergi

Author (s): Kaya Onur Dag

Title: Modification of airfoil characteristics due to the influence of the free vortices in the wake of a rotor

Department: Department of Wind Energy

DTU Wind Energy Master Thesis
M-0026
September 2013

Technical University of Denmark
Department of Wind Energy
Frederiksborgvej 399
Building 118
4000 Roskilde
Denmark
www.vindenergi.dtu.dk

Contents

List of Figures

Acknowledgments

First of all, I would like thank my supervisor Jens N. Sørensen for offering me such a research project. I found myself inside the topic instantly and was motivated enough to spend hours on it without bothering. I believe that I wouldn't be as motivated as I was with another project. I also appreciate his time and suggestions for pushing me to reach concrete results and conclusions. He always kept feeding me with valuable information and questions which added curiosity on my project and became the main motivation source for myself. Moreover, I would also like to thank him for creating such a free atmosphere for me where I was able to apply my own thoughts and adjust the direction of the solution.

I am also thankful to Emmanuel S. P. Branlard who spent his time on discussions with me on numeric implementations of the methods that I used in this work. Moreover, I also appreciate Néstor R. García' s help where he spent his time on running simulations with his panel code for my comparisons. Without his help, I wouldn't be able to have reliable conclusions.

I would also like to thank to my colleague Emre Barlas who spent his time on reviewing my report.

Abstract

In this work, the change of the airfoil characteristics due to the influence of the wake will be presented. The main influence from the wake was observed at the tip regions where the induction changes along the chord. As a result of this the lift decreases. The effect is explained with detailed figures[1] throughout this thesis.

The simple and rapid calculation method, Blade Element Momentum theory, which is being used frequently by the industry disregards this lift drop, which will be referred as *decambering*. To be able to use 1-D momentum theory, which assumes to have infinite blades, together with the well known finite blade approach, blade element method, tip corrections are introduced. Tip loads are being wiped out with this implementation. As a result of this, the disregarded decambering error assumed to be minimized yet not canceled out.

This report makes different approaches to calculate the lift drops with respect to chordwise induction changes due to tip and trailing vortices which are released between each spanwise station. The calculations in this work were based on lifting line and panel method solutions which are explained in the following chapters. For this purpose, a panel and a lifting line code were developed with prescribed and free wake modeling for both.

The main approach to the problem was to find induction distribution on each cross-section and represent the lift drop in terms of either angle of attack or C_L. For this purpose, thin airfoil theory was used and representation was done with a $\Delta\alpha$ value as an angle of attack correction.

At the end, it was concluded that the decambering effects yield to considerable drops in circulations at the tip regions.

[1]The sketches and plots used in this paper were drawn or generated by the author. Reproduced figures are also referenced.

Chapter 1

Introduction

The most well-known wind turbine rotor calculation methods are the lifting line approach and the Blade Element Momentum theory. Both of these methods rely on the blade representation as a line on the one-quarter chord points on each cross-section.

In both of these methods, and in any other blade-element based rotor calculation techniques such as actuator line, the angle of attack for each cross-section region is calculated at one-quarter chord and forces are found with respect to this value. The induced velocities for lifting line is calculated from the trailing vortices with respect to the one-quarter chord point whereas for the BEM and actuator line techniques, the induction is either taken from the 1-D momentum or a flow solver. However, these approaches yield to an error due to the effect of vortices which causes a chordwise flow direction change on the cross-section. The representation is shown in Fig1.1.

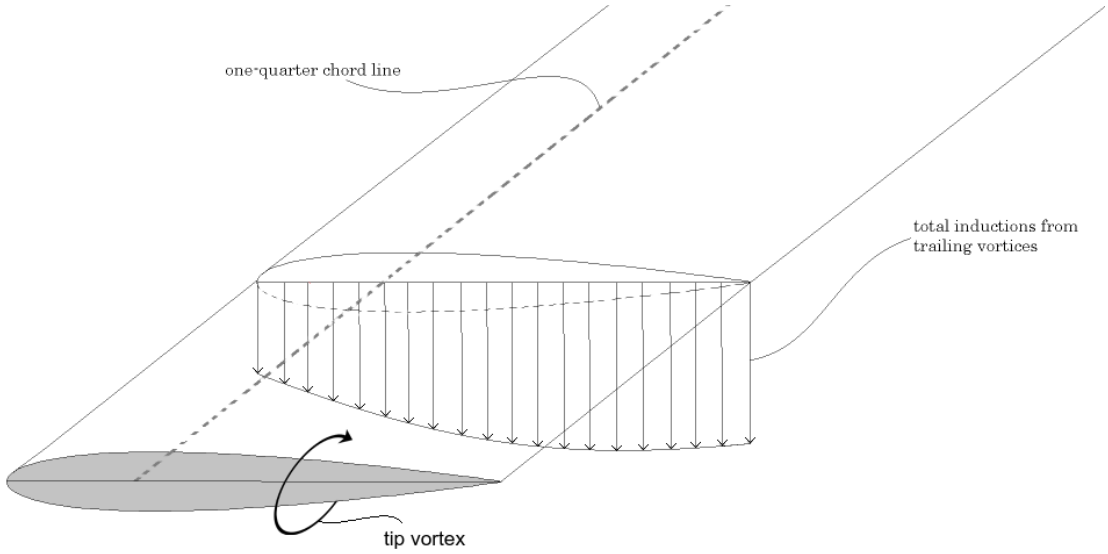

Figure 1.1: Induction change close to tip region

1.1 The Physical Phenomena Behind The Angle of Attack Change

The two main physical causes are the well-known tip vortex and trailing vortices. Simple background of these can be found in the following sections.

1.1.1 Tip Vortex

In aerodynamics, the lift force is generated from the pressure difference between two sides of the airfoil surface. The low pressure side called the suction side, which is the lift direction and the other part called the pressure side. At the middle regions of a wing, pressure differences of these two sides generates pure lift. However, around the tips of the wing, the pressure difference tries to vanish itself and generates a spanwise pressure gradient which causes leakage from pressure side to upper suction side at the tips. As a result of this behavior, well known tip vortex is being generated and starts convecting downstream and starts to roll-up(see the Fig.1.2). Moreover, this leakage effect also erodes the generated pressure difference and hence the magnitude of the lift force dramatically decreases.

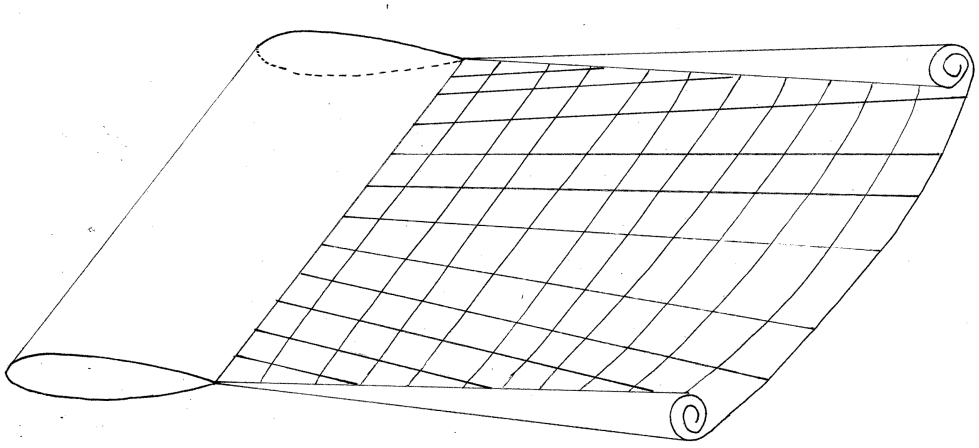

Figure 1.2: The vortex sheet being released from a planar wing

1.1.2 Trailing Vortices

As a result of generated spanwise pressure gradient, at the pressure side a new velocity component towards the tip occurs. Similarly on the suction side another velocity component occurs, this time towards the middle of the wing. When the flow from the two surfaces reaches the trailing edge, these two components generates vortices which will be convected through downwind. This vortex sheet is formed at the trailing edge and

for this reason will be called as trailing vortices [1]. Moreover, although it is known that tip vortices start forming before the trailing edge at the very edge of wing, they can also be considered as trailing vortices.

1.1.3 Effect of Vortices

According to the industry standard Biot-Savart Law, which was found by two scientists named Jean Baptiste Biot and Felix Savart in the first quarter of the 19^{th} century, magnitude of the induction generated by a vortex is inversely proportional to the distance between the point of induction and vortex core center [1]. As a result of this, the closer the point the higher the induction from the corresponding vortex.

For wing calculations, for instance for lifting line method, the induction point for angle of attack calculations are chosen to be the one-quarter chord which is the known pressure center of lifting surface. However, inductions at one-quarter chord point is not constant through the chord. Due to starting trailing and tip vortices, the inductions close to the trailing edges are stronger than the ones at the leading edge. As a result of this difference, flow draws an uncounted arc through the downstream chord due to increased induction. Due to the direction change in the flow, angle of attack varies.

1.2 Historical Context

In 1995, *Bjorn Montgomerie* handled this issue in his article named '*Explanation of an effect of lift reduction near the tip caused by the local flow around airplane wings or wind turbine tips* [6]. In his article the whole phenomena is covered despite the fact that the provided results were not satisfactory. In that work, the cause was clearly explained and an approach with trailing vortices to solve the issue was carried out. However, due to unsteady iterations in angle of attack change at the tip regions, where the effect is mainly considered, the results were not gratifying.

1.2.1 Naming The Effect

The induction change can be seen from the Fig.1.3. From leading edge to the trailing edge, flow is being bent or in other words, runs away from the surface, regardless of the bound vortex. This is not a physical scenario for a wind tunnel experiment or a numeric 2-D airfoil lift calculation which are both used to determine lift coefficients for corresponding geometrical angles of attack.

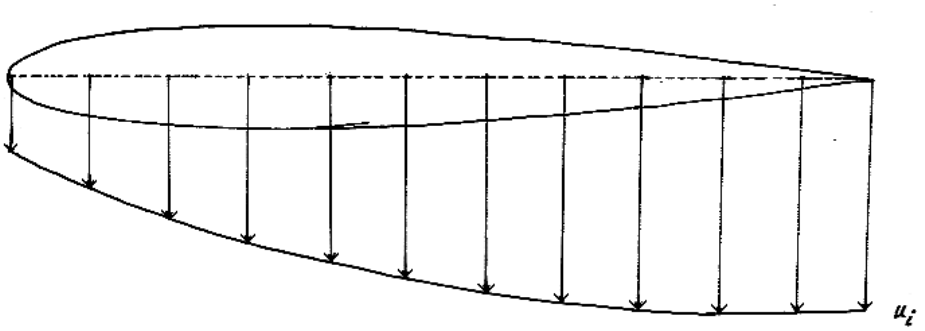

Figure 1.3: Downwash from the trailing vortices[6]

In order to aerodynamically model this behavior, Montgomerie came up with an idea of adding negative bending, upside-down cambering to the airfoil and assuming a flat, non-bent flow instead. The representation is shown below in Fig.1.4. Instead of modeling a complicated bent flow with the actual wing geometry, taking the negative camber into consideration and changing the geometry for modeling part was. The representation of the negative bent chordline, named as *Decambering* by Montgomerie, is shown in Fig.1.4.

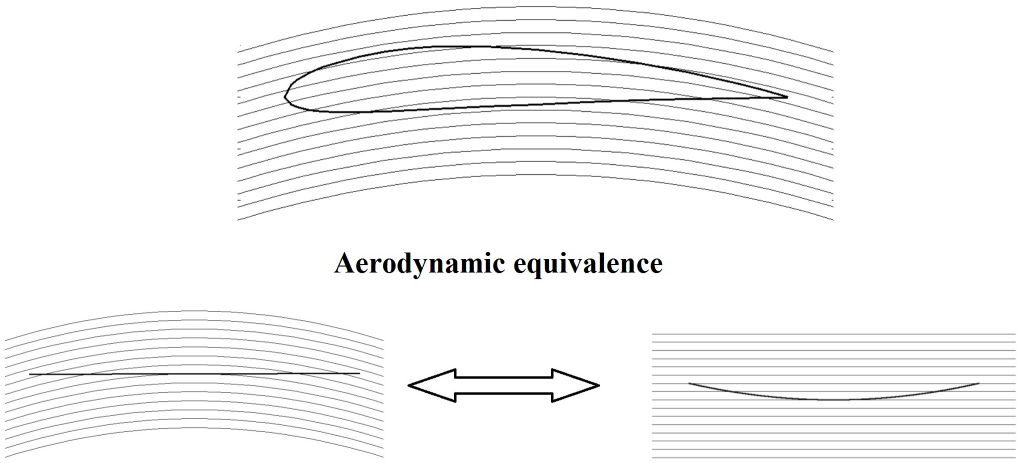

Figure 1.4: Aerodynamically representation of bent flow [6]

With decambering, 2-D aerodynamic calculations could easily be proceeded with having 3-D effects in consideration with usage of thin airfoil theory.

In his studies, Montgomerie calculates the zero lift angle of attack C_{L0} for decambered chordlines and uses this as a correction to the actual angle of attack. With respect to the found angle, he calculates the new circulations and dropped loadings. Due to lowered circulations, trailing vortices should also be decreased their strength and as a result of

this, decambering changes again. With respect to this issue, this approach should be carried out with iterations. However, in his work due to increased irregularities and non-converged values at the tip regions, iterations could not be proceeded. Nevertheless, Montgomerie claimed that the first order effect of this approach would work fine since there were very little effects recorded at the middle regions with iterations.

1.3 Basic Concepts

In this section a general description of the methods and phenomenas are briefly explained in order to gain familiarity. Thereby the vortex methods which are implemented in this thesis can be seen from a broader perspective.

1.3.1 Modeling Methods

For aerodynamic calculation of a lifting device, there are many different techniques which vary dependent on the purpose. These methods can be grouped under three main titles.

2-D based methods

These can be considered as the ones that on airfoil polar curves taken by 2-D data such as wind tunnel experiments or two dimensional numeric computations such as Xfoil[1]. The industry standard blade element theory for wind turbines is a good example to these methods. Simply, blade geometry and aerodynamic properties at every spanwise station are used to determine the lift and drag forces with an assumption of two dimensional flow behavior at each element.

The main advantage of these methods, without a doubt, their very low computing cost which becomes extremely handy for the design part and life time aeroelastic simulations. However, despite the rapidity of these methods, the appearance of 3-D effects make these simulations unreliable. The majority of the research conducted in this area is related to the understanding of flow behaviors and developing empiric or semi-empiric relations for consideration of these neglected effects in rapid calculations.

A very good example can be the tip corrections being used with BEM methods to fix the less realistic actuator disk assumption in 1D momentum theory. 1-D momentum theory is used for taking the wake effects in 2D blade element calculations yet the theory assumes the wind turbine rotor as an actuator disk with a constant thrust loading which is not the reality for a finite number bladed wind turbine.

[1] A well-known software for the design and analysis of subsonic airfoils.

The accuracy of these methods are based on the adequacy of used corrections, or in other words representations, for non-modeled 3-D effects.

CFD Methods

CFD solutions are usually the most costly and the most realistic ones. In a full scale DNS simulation, an appropriate mesh can cover every aspect of a fluid flow around the object, turbine rotor, blade or an airfoil. However, for instance, a full scale wind turbine DNS simulations can not be yet proceeded due to massive amounts of required computing power for any reasonable Reynolds number. Instead, turbulence model based CFD simulations are being used such as well known RANS or LES[2]. In these turbulence models, simply the small scale eddies are represented by introduced models and cost being decreased significantly due to increased mesh size for corresponding Reynolds value.

The rotor calculations can be carried out with full scale CFD computations. In addition, relatively easier approaches such as actuator disc, actuator line can be employed for decreasing the computational cost in a less detailed manner. However, as aforementioned, these methods lead the way to the 2-D based polar data which again results with neglected 3D errors on airfoil characteristics.

Vortex Methods

Vortex methods are based on induction calculations with Biot-Savart Law. Simply, the geometries are represented by vortices and calculations are done by satisfying the required boundary conditions regardless of viscous effects. These are often used for aircraft calculations and ready-to-use codes are available such as Xflr5[3] under GNU General Public License[4].

In general, although it very much depends on the modeled object and the wake domain, the cost of vortex methods are usually lie between CFD simulations and simple 2D based models. The lower cost in comparison with CFD methods is due to the fact that the modeling part in vortex methods is mainly the geometry and the wake instead. With these methods, complex geometries can be modeled easily. On the other hand, for a CFD simulation, boundaries needs to be handled carefully with finer meshes for complex parts which causes a dramatic increase in simulation costs.

There are several types of vortex methods for different purposes. The airfoil representation with different methods are illustrated below in Fig.1.5.

[2]Turbulence models:Reynolds Averaged Navier Stokes, Large Eddy Simulation

[3]An analysis tool for low Reynolds planes with lifting line, vortex-lattice, surface panel codes inside

[4]A free, copyleft license for software and other kind of works

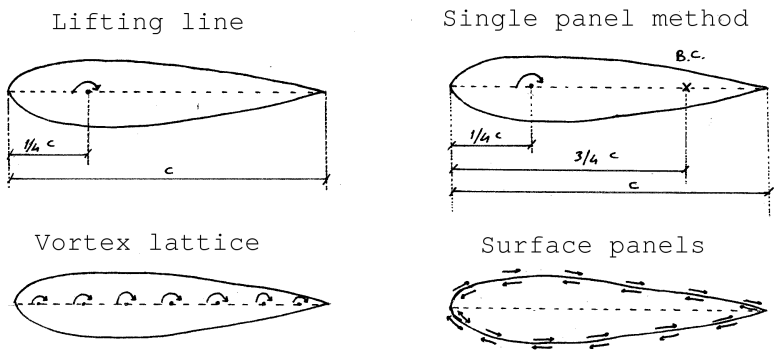

Figure 1.5: Illustration of different vortex methods

Apart from wing representation, the wake also needs to be modeled. Two main model types are called prescribed and free wake. As its name implies, a prescribed wake is a pre-defined wake geometry where the vortex coordinates are known before the simulation starts. The geometry of the wake can be updated in parallel with the simulation with respect to the inductions or kept fixed. The free wake, on the other hand, is the wake model where the vortices are being released from the trailing edges and convected downwind with respect to the inductions from other vortices and free stream velocity. The free wake, surely, is a better representation of the reality yet the computational cost is relatively expensive in comparison with a prescribed model. To decrease the cost for a free wake simulation, some techniques can be applied such as using a free wake in the near wake region and modeling far wake region with prescribed wake or sophisticated methods such as fast multi-pole accelerated free wake can be implemented [4].

1.3.2 Angle Of Attack

Although it sounds rather simple by name, it actually is quite complex when it comes to the data transfer between different methods where the same language is not being used. It is important to emphasize the differgmaences in terms of angle of attack observation between the aforementioned models and recall the cause of this effect.

Wind Tunnel

When we recall a wind tunnel test section, as known, the angle of attack is simply taken by the geometry.

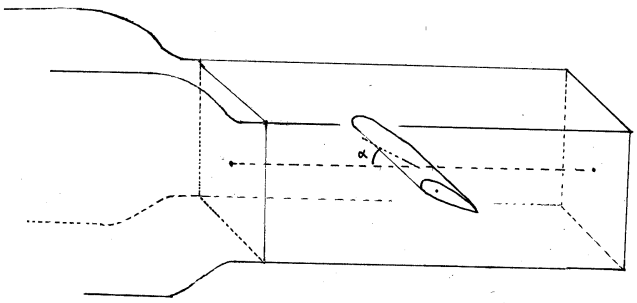

Figure 1.6: A sketch of a wind tunnel measurement

The angle being taken into account is the angle between the free stream axis and the chordline of the attached wing section. Due to the boundaries of the wind tunnel, there are no tip or trailing vortices being generated as a result of having almost constant circulation through the span.

Lifting Line

In a lifting line simulation, the angles of attack are calculated with respect to the geometry plus the total induction (u_i) being calculated at one quarter chord point. The illustration of the method is shown below in Fig.1.7. The main difference between wind tunnel measurements is the induction factor which is the part where the trailing vortices are considered.

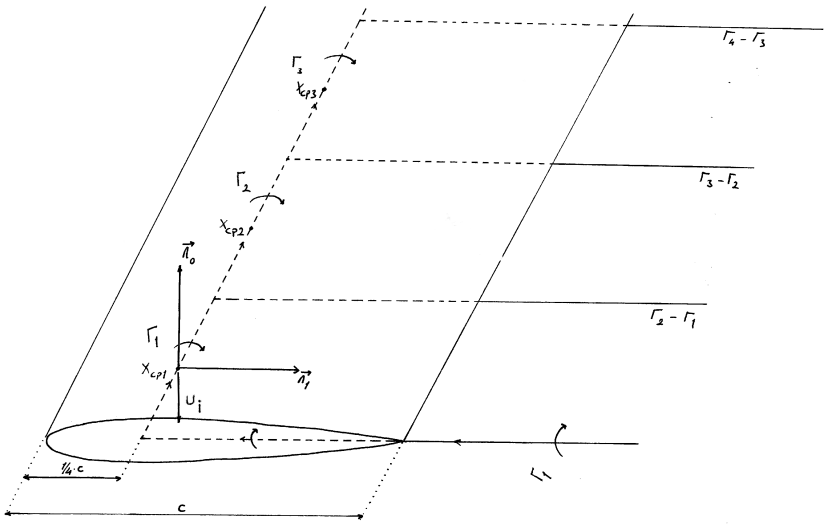

Figure 1.7: Illustration of the angle of attack calculation for a lifting line technique

At the middle regions, the inductions are almost zero where the effect of trailing vortices

are rather small. As a result of this, the angle of attack becomes purely geometrical as it is in a wind tunnel. At the tips, however, due to strong trailing and tip vortices, the angle of attack is always smaller than the geometrical value which is being handled by the quarter chord inductions in lifting line method.

Single Panel Method

The simple representation of the panel method with its control point at three quarter chord point is shown below.

The single panel method is

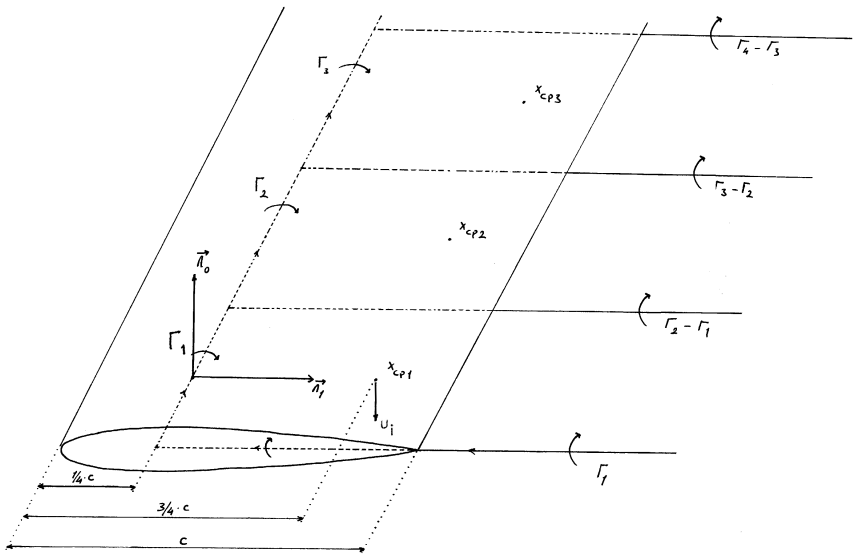

Figure 1.8: Illustration of the angle of attack calculation for a single panel method

Although the idea is quite similar, the angle of attack calculation is based on the induction at quarter chord point with Kutta condition which will be clarified in detail in the next chapter. As a result of having three quarter control point, the effect from trailing vortices are stronger thus the angles of attack from a lifting line and a single panel method are inconsistent.

1.4 An Outline of the Report

The contents of this report is organized as follows. Chapter 2 presents the calculation of the effect and explains the approaches being handled. The application of change methods are presented on a non-rotating planar blade. Chapter 3 then describes practical application to a planar wing and a rotating blade with lifting line and single panel

methods. In Chapter 4, application of suggested method to the MEXICO turbine with BEM method is presented and results are discussed in detail. Furthermore, validation with a free wake full surface panel code is shown. The conclusions are then summarized in Chapter 5.

Chapter 2

Description of the Model

The general description of the problem and modeling approach is given in Fig.1.4 and Fig.1.1. As aforementioned, the cause of decambering is the inductions from trailing vortices which are considered as wake. Thus, vortex based calculation methods were employed to find a way to take this 3D effect into account in 2D based calculations. The decambering effect is already being accounted in vortex methods where the camberline is handled with more than a single point representation such as vortex lattice or surface panels (see the Fig.1.5). Since the main motivation for this project was to find a way to model this in 2D based methods, such as blade element and actuator line technique which is commonly used for sophisticated CFD simulations, single point methods were selected for similarity and simplicity.

2.1 Modeling the Lifting Surface

For bound vorticity calculations, lifting line and panel method were employed to calculate circulation distributions for both planar wings and turbine blades being calculated in this paper.

In both of these methods, the surface is assumed to consists of discretized horseshoe vortices where the middle vortex lines, called the bound, fixed at one quarter chord line. In the Fig.2.1, a planar wing is shown for illustration.

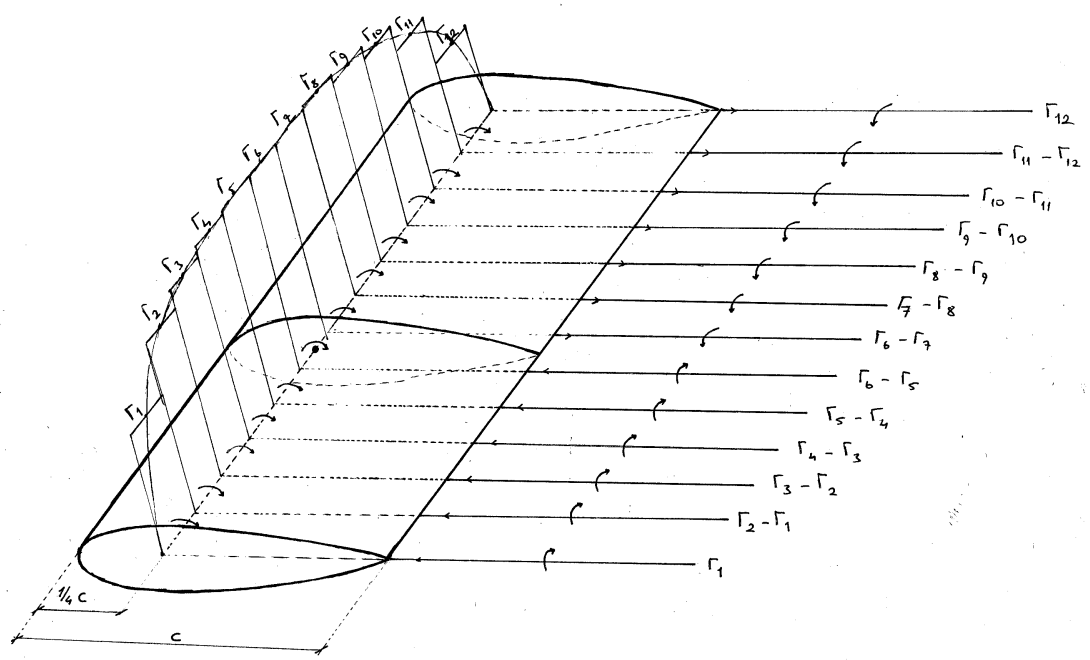

Figure 2.1: Wing representation with circulation strengths

For the wing being handled in the Fig.2.1, the surface is divided into twelve spanwise stations where each of these corresponds to a circulation magnitude, Γ.

2.1.1 Lifting Line Model

To model such a wing with a lifting line technique, inductions needed to be taken at one quarter chord point from all the vortices for every spanwise station. The induction calculations were done with Biot-Savart Law as shown in eq.2.1[9]. A vortex core model could also be employed. Nonetheless, to keep the simplicity, this wasn't considered. Detailed information for vortex core models, application results and their comparison can be found in the references [8].

$$\vec{u_\Gamma}(x_p) = \frac{-1}{4\pi} \int \Gamma \frac{\vec{r} \times \vec{dl}}{r^3} \tag{2.1}$$

When we apply this equation to a line vortex as shown in Fig.2.2, and take the integration, the expression becomes as shown in eq.2.2 [9].

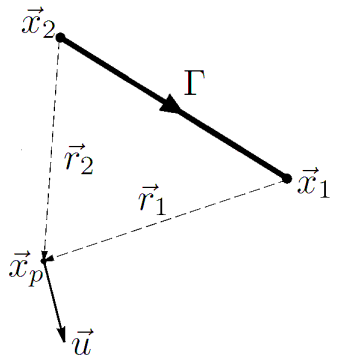

Figure 2.2: Vortex line

$$\vec{u_\Gamma}(x_p) = \frac{\Gamma}{\pi} \frac{(r_1 + r_2)(\vec{r_1} \times \vec{r_2})}{r_1 r_2 (r_1 r_2 + \vec{r_1} \cdot \vec{r_2})} \tag{2.2}$$

where $\vec{u_\Gamma}(x_p)$ is the induction vector at the point x_p from the vortex Γ_{x_1,x_2}. With this equation, inductions at quarter-chord points can be calculated from each vortex line and summation will give the total induction.

In the Fig.2.1, the spanwise discretization is drawn with equal distances to keep the simplicity. However, for calculations, full *cosine* distribution of spanwise stations and control points was used.

On the other hand, the wake is handled with a prescribed geometry for all the simulations. To find the strengths of circulations in the wake, $\Delta\Gamma$ is considered between each spanwise stations as shown in Fig.2.1.

To obtain the circulations at each one quarter station point, the angle of attack was calculated. Procedure of angle of attack determination is shown below.

$$\alpha = tan^{-1}\left(\frac{\vec{V_\infty} \cdot \vec{n_0} + \sum_{i=1}^{N}(\vec{u_i} \cdot \vec{n_0})}{\vec{V_\infty} \cdot \vec{n_1} + \sum_{i=1}^{N}(\vec{u_i} \cdot \vec{n_1})}\right) \tag{2.3}$$

where α is the angle of attack, $\vec{V_\infty}$ is the free stream velocity vector, $\vec{n_0}$ and $\vec{n_1}$ are surface normal and chordwise directions respectively. The induction u_i can be defined from the eq.2.1.

With respect to the found angle of attack, lift coefficient C_L and drag coefficient C_D can easily be taken from lift/drag coefficient tables. Although, vortex methods are based on inviscid flows, lifting line technique allows us to use viscous data from wind tunnel or viscous CFD simulations. To obtain the circulation distribution, *Kutta-Joukowski Theorem* is used for the relationship between lift and the circulation. The definition is

shown below.

$$\Gamma = \frac{L}{\rho V_\infty} \tag{2.4}$$

where L is the lift force acting on the lifting surface and the Γ is the circulation. More details about this theorem and derivation can be found in ref.[5].

With resulted circulation distribution, trailing vortices can be found by taking the differences between bound circulations as shown in the Fig.2.1.

In this iterative procedure, only the one-quarter chord inductions are taken into account for determining the flow angle which is not a problem for the middle regions where trailing vortices are insignificant. Nevertheless, at the tip regions, inductions from trailing vortices become effective on angle of attack. Moreover, the inductions at the trailing edges are relatively larger than the ones at the quarter-chord points due to distance to the wake vortices. The total induction through the chordline varies. Thus, angle of attack change is clearly seen on the chordwise direction.

2.1.2 Panel method

Another single point vortex method where the bound vorticity is fixed at one quarter chord point as same as lifting line, called panel method. In order to avoid misunderstanding the method will be referred as *single panel method* as shown in Fig.1.5. In this method, the circulations are found by solving closed equations with respect to three quarter chord collocation point, called the Kutta condition. Representation and collocation point is shown in Fig.1.8 in previous chapter.

The Kutta condition is a principle of having zero-penetration through the chordline.

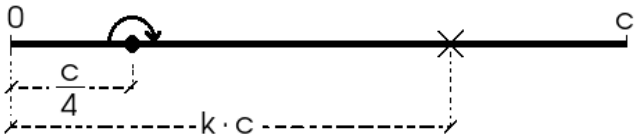

Figure 2.3: Flat plate single panel method representation [5]

If we represent the lifting flat plate with a single vortex which is fixed at the center of the pressure, one quarter chord, the boundary condition requiring zero normal flow at the surface can be specified at a single point. Assuming that this point is at a distance $k \cdot c$ along the chordline from the leading edge (see the Fig.2.3), the boundary condition with zero velocity can be found via;

$$\frac{-\Gamma}{2\pi[kc-(1/4)c]}+Q_\infty\alpha=0 \tag{2.5}$$

where the Γ is the circulation at quarter chord point, Q_∞ is the free stream velocity and α is the angle of attack.

The circulation of a flat plate is represented as

$$\Gamma=\pi cQ_\infty\alpha \tag{2.6}$$

When we substitute this inside the eq.2.5 the collocation point becomes

$$k=\frac{3}{4} \tag{2.7}$$

which represents the distance from the leading edge [5].

In this method, sum of the velocity components induced by the wing and wake vortices, plus the normal velocity component of the free-stream flow must be zero on the collocation point. With this introduced boundary condition, equations are closed for every spanwise station and one unique solution for circulations can be obtained with respect to the inductions taken at three-quarter chord point at each every station.

2.2 Circulation Differences at Tip Regions

Panel method solution of a simple planar wing is expected to get more influence from the trailing vortices, which results as non-equal circulations at the locations where trailing vortices are relatively strong.

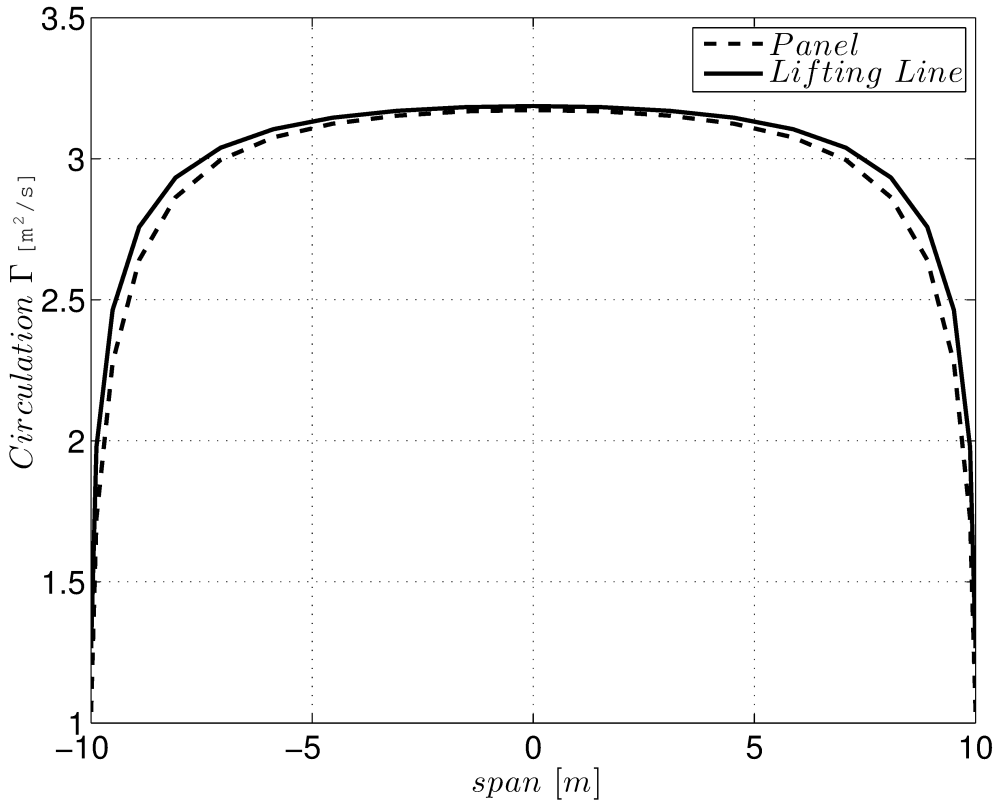

Figure 2.4: Panel vs. lifting line

The Fig.2.4 presents the circulation distribution through the spanwise stations for a planar wing with 1 meter chord and an aspect ratio of 20. The airfoil profile was chosen to be the NACA0012. Since the panel method is not capable of modeling the thickness effects, the lift coefficient curve is obtained by $C_L = 2\pi\alpha$ where α stands for angle of attack for a flat, zero-thickness plate.

As seen from the plot, at the middle regions the circulation strengths are the same. However, close to the tip regions, lifting line circulations are larger than the ones that are calculated with panel method.

As aforementioned, the flow bends through the chordline at the tip regions and as a result of this, angle of attack decreases. Since the control point of the single panel method is more downstream and closer to the trailing vortices, it results with a smaller angle of attack, which leads to smaller circulations.

In Fig.2.5 total inductions on normal direction on the wings surface by the wake is shown. It can easily be concluded that, induction change through the chord is almost none in the middle regions where the one-quarter and three-quarter inductions are almost the same. On the other hand at the tips, increased induction along the chordline causes uneven circulations between the panel and the lifting line solutions due to discrepancy between angles of attack.

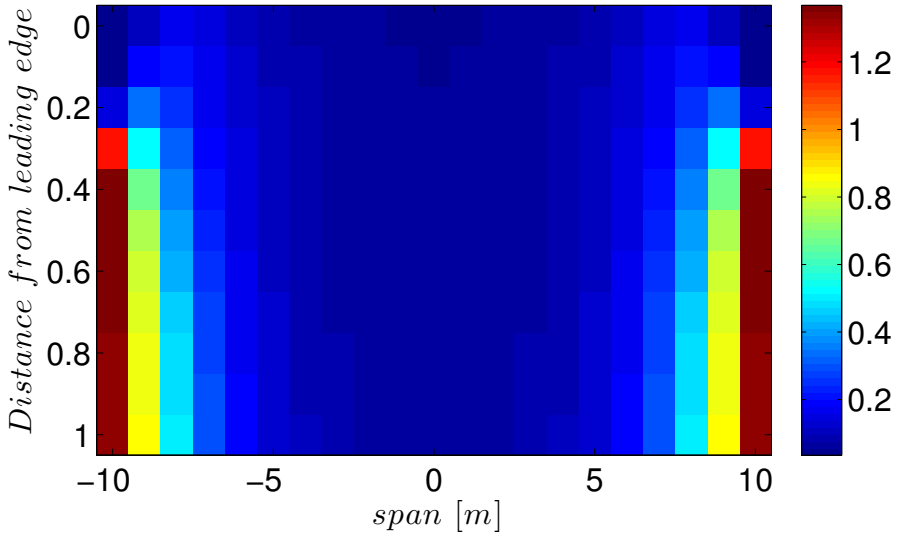

Figure 2.5: Inductions $[m/s]$ on the wings surface. $V_\infty = 8[m/s]$, $\alpha = 5°$

With this information, it can be said that decambering clearly exists and not being taken into account in 2D based models.

In the next section, different approaches will be elaborated in detail to model the effect. The main aim will be, as in the first chapter, to calculate the aerodynamic properties of changed geometry due to decambering effect.

2.3 Modeling the Decambered Camberline

This part will be handled under two main titles. First, the panel method, which is considered as more desirable compared to the lifting line approach in terms of decambering, will be taken as a base line point and suggestions will be made to be able to reach its results from lifting line solutions. The cons and pros of this approach will be discussed in detail.

As shown before, panel method takes the flow angle into account only at three-quarter point. Yet, on the other hand, considering the full induction change along the chordline is a robust way of dealing with decambering for a specific local section. In the second part, two different approaches for full induction changes and corresponding decambering effects will be presented.

2.3.1 Approach to Single Panel Method Results from Lifting Line

The simplest and the most straight forward approach would be to find panel method results, subtract them from lifting line circulations and call it a correction which would work as an add-on for 2D based models. However, reality is not that straight forward.

First of all, single panel method is a method where the lifting surface is assumed to consists of a flat plate where thickness and the camber effects are canceled. Simply, it can not be used for a wing with cambered airfoil profiles.

Secondly, since this correction is aimed to be applied on 2D based models, it wouldn't make much of a sense to run two extra different kinds of simulations with heavy wake calculations in them in order to apply a correction to a method which only needs seconds to simulate the rotor, such as BEM.

With consideration of these statements, the first attempts was to try to calculate the difference between these two techniques analytically.

The step-by-step lifting line calculation procedure is shown below.

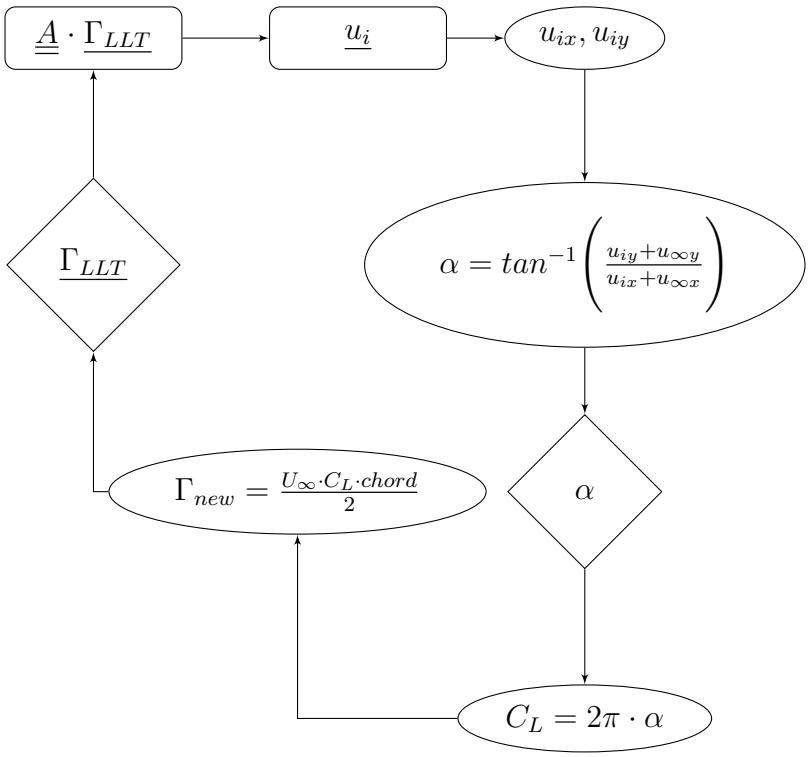

Figure 2.6: Lifting line iterative procedure

In the Fig.2.6, u_i is the inductions and $u_{ix,y}$ represent the induction on chordwise and on the normal direction respectively for every spanwise station, α is the angle of attack, and A is the influence matrix which is being generated via Biot-Savart Law with respect to the control points at one-quarter chord.

As seen, lifting line approach is an iterative process where the system converges to a circulation value as a result of changed angle of attack.

Nevertheless, on the other hand, the single panel method which is shown below in eq.2.8, is a closed equation system which leads to a one-shot solution for circulations.

$$\underline{\underline{A_p}} \cdot \underline{\Gamma_p} = \underline{-u_\infty y} \tag{2.8}$$

In this system, which satisfies the Kutta condition, $\underline{\underline{A_p}}$ is the influence matrix for panel method for calculating inductions on normal direction at three-quarter chord points, $\underline{\Gamma_p}$ is the circulation vector and $\underline{u_\infty y}$ is the normal direction component of the free stream velocity at three-quarter point.

If we write the system down for a single station control point;

$$A_{11}\Gamma_{p1} + (A_{12}\Gamma_{p2} + A_{13}\Gamma_{p3} + ... + A_{1N}\Gamma_{pN}) = -u_{\infty y(1)} \tag{2.9}$$

By calling the part in parenthesis x_1 the system becomes;

$$A_{11}\Gamma_{p1} + (x_1) = -u_{\infty y(1)} \tag{2.10}$$

where the Γ_{pi} is the circulation from panel method for the spanwise station i.

If we write the whole system down;

$$\underline{\underline{A^*}} \begin{bmatrix} \Gamma_{p1} \\ \Gamma_{p2} \\ \Gamma_{p3} \\ : \\ \Gamma_{pN} \end{bmatrix} = \begin{bmatrix} -u_{\infty y1} \\ -u_{\infty y1} \\ -u_{\infty y1} \\ : \\ -u_{\infty yN} \end{bmatrix} - \underline{\underline{X}} \begin{bmatrix} \Gamma_{p1} \\ \Gamma_{p2} \\ \Gamma_{p3} \\ : \\ \Gamma_{pN} \end{bmatrix}$$

where

$$\underline{\underline{A^*}} = \begin{bmatrix} A_{11} & 0 & 0 & ... & 0 \\ 0 & A_{22} & 0 & ... & 0 \\ 0 & 0 & A_{33} & ... & 0 \\ : & : & : & & : \\ 0 & 0 & 0 & ... & A_{NN} \end{bmatrix}$$

and

$$\underline{\underline{X}} = \begin{bmatrix} 0 & A_{12} & A_{13} & ... & A_{1N} \\ A_{21} & 0 & A_{23} & ... & A_{2N} \\ A_{31} & A_{32} & 0 & ... & A_{3N} \\ : & : & : & & : \\ A_{N1} & A_{N2} & A_{N3} & ... & 0 \end{bmatrix}$$

When we leave the Γ_p on the left alone, system becomes;

$$\underline{\Gamma_p} = -\frac{\underline{\underline{u_{\infty y}}} + \underline{\underline{X}}\ \underline{\Gamma_p}}{\underline{\underline{A^*}}} \tag{2.11}$$

On the other side, we can write an equation for circulation from the lifting line technique for a known induction for each spanwise station .

$$L = \frac{1}{2}\rho dA u_\infty^2 C_L \tag{2.12}$$

where L is the lift force generated from the airfoil section with and area of dA and lift coefficient of C_L. From the Kutta-Joukowski Theorem, lift force being generated from a vortex line can be written as below.

$$L_\Gamma = \rho \Gamma u_\infty l \tag{2.13}$$

where l is the length of the vortex line with a strength Γ.

When we merge these two equations, we end up with circulation expression which is used in lifting line technique.

$$\Gamma = \frac{u_\infty C_L c}{2} \tag{2.14}$$

where c is the chord length of the corresponding spanwise station.

With an assumption of inviscid flow and flat plate as an airfoil, we can simplify the C_L as $2\pi\alpha$ where α is the angle of attack in radians and can be taken as $\alpha = tan^{-1}\Big(\frac{u_{iy}+u_{\infty y}}{u_{ix}+u_{\infty x}}\Big)$. If we put these expressions in to the eq.2.14, we end up with expression shown below for circulation magnitude from lifting line.

$$\Gamma_{LLT} = u_\infty c\pi tan^{-1}\Big(\frac{u_{iy}+u_{\infty y}}{u_{ix}+u_{\infty x}}\Big) \tag{2.15}$$

where the u_{iy} and u_{ix} can be written as $A_y\Gamma$ and $A_x\Gamma$ respectively.

From the subtraction of panel method from the lifting line with the eq.2.15 and eq.2.11, expression for $\Delta\Gamma$ occurs.

$$\Gamma_{LLT} - \Gamma_{panel} = \Delta\Gamma = u_\infty c\pi tan^{-1}\Big(\frac{\underline{\underline{A_y}}\underline{\Gamma_{LLT}} + \underline{\vec{u_\infty}\cdot\vec{n_0}}}{\underline{\underline{A_x}}\underline{\Gamma_{LLT}} + \underline{\vec{u_\infty}\cdot\vec{n_1}}}\Big) \; + \; \frac{\underline{\vec{u_\infty}\cdot\vec{n_1}} \; + \underline{\underline{X}}\underline{\Gamma_{panel}}}{\underline{\underline{A^*}}} \tag{2.16}$$

where the X stands for induction matrix A with zeros in the diagonal and A^* is the matrix A only with diagonals as shown before.

As seen from the eq.2.16, $\Delta\Gamma$ is still dependent on Γ_{panel}. However, the multiplier of Γ_{panel} is the X which is A influence matrix for panel method with zeros on the diagonal. The matrix A is in a diagonally dominant form as a result of having the closes trailing vortex from the same station. Due to zero diagonal, it can be said that multiplication of X either with Γ_{panel} or Γ_{LLT} wouldn't change the result much.

When this method was implemented, the equation system can be closed with known Γ_{LLT}. Moreover, with this way, cambering effects could also be taken into account for the correction part with corresponding C_L data with introduced lifting line circulations instead of panel method.

The numeric implementation of the system showed that the system actually works well for small numbers of discretized spanwise stations, nonetheless, with the increased control points, the matrix A becomes less effective on its diagonal and the error in the $\Delta\Gamma$ reaches to unacceptable values. Even though the results with less than 6 spanwise stations were reasonable in terms of circulation correction, such a coarse discretization is quite far away from a good representation of the wing, rotor blade or simply a lifting surface.

Considering this fact, it was concluded that there is no easy way to correct lifting line with a simple expression to reach single panel method values.

2.3.2 Full Induction Variety Calculations

Until this part, panel method was considered as more appropriate than lifting line. However, although panel method has a better representation of decambering with three quarter collocation point, it still is a single-point-based model. In order to have a tailored cut model for decambering, it was a necessity to handle the whole chordwise induction change instead.

It was known that the flow direction change could be represented with shape change of the airfoil section and resulting aerodynamic forces would be the same. In order to do this representation, flow path had to be found. For this purpose, the chordlines in each spanwise station are divided with 11 equal-distance control points and inductions were calculated up on them. With respect to these calculations, the flow path can easily be found at each control point.

The trailing vortices induced trajectory of a flow passing through a wing with an 8 meter span and 1 meter chord length planar wing is shown in Fig.2.7. It is important to mention that the trajectory shown here is not the real streamline direction where the bound vortices also act on the flow. The figure represents the disregarded effect in 2D wind tunnel experiments.

As seen, at the middle regions, effect of trailing vortices are relatively small whereas at the tip regions, the effect is considerably large and changes the flow direction dramatically.

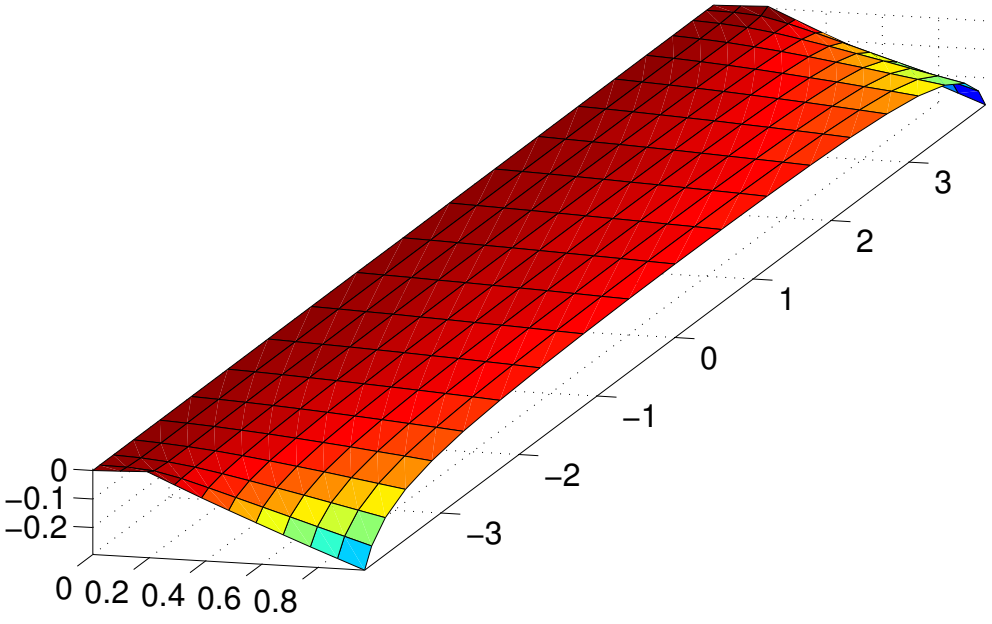

Figure 2.7: Trailing vortices induced trajectory of a flow on the chordline of a wing, AR=8

In order to aerodynamically model this physical behavior, as aforementioned, the flow trajectory change had to be transferred to the chordline in negative direction. However, the one-quarter chord inductions are already taken into account in lifting line solution thus, the induction at one-quarter chord point is subtracted in each spanwise station. The resulting flow trajectory is shown in Fig.2.8.

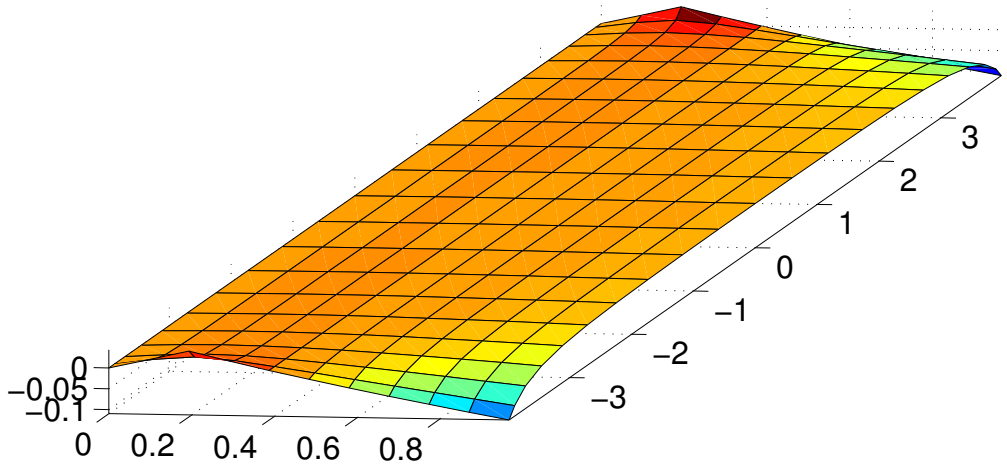

Figure 2.8: Trailing vortices induced trajectory with subtracted one-quarter induction

Simply, for aerodynamic calculations, this trajectory can be transferred to the corresponding airfoil section in the negative direction and aerodynamic forces will be the same as with the case where the trailing vortices does not bend the flow. The decambered chordlines are shown in Fig.2.9.

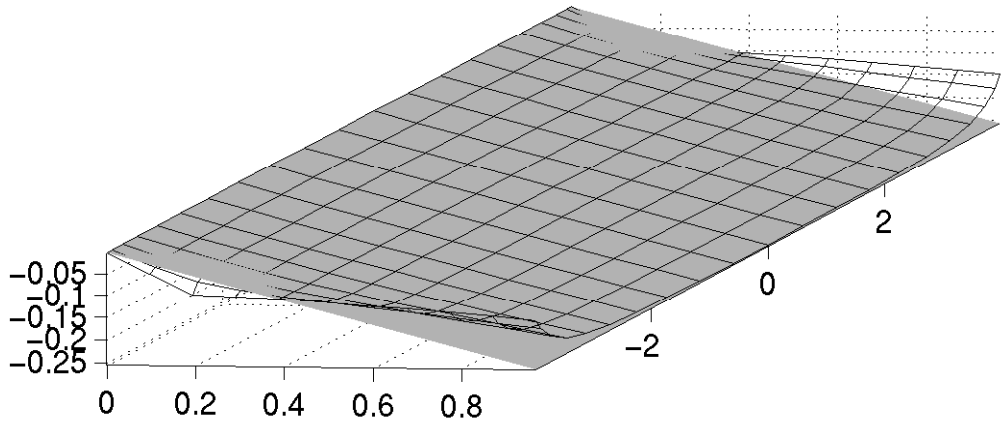

Figure 2.9: Decambered chordline(meshed) and the actual camberline(grey)

In Fig.2.9, the grey area is the chordline of a NACA0012 wing with an aspect ratio of 8 and the gridded surface is the decambered wing which decreases its angle of attack

through the trailing edge at the tip regions. The original and decambered shape of the half wing is shown below in Fig.2.10.

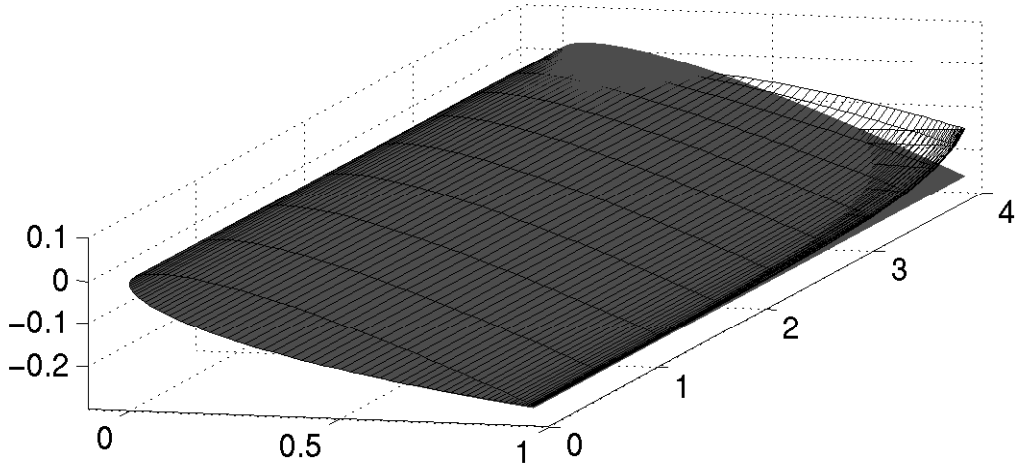

Figure 2.10: Right side of a NACA0012 wing with(meshed) and without(grey) decambering effect starting from the middle towards tip

From this point, the challenge was to be able to represent the new shape in terms of C_{Lnew} or α_{new}. As a result of having a bent chordline, it was not possible to find a linear chord line which would easily be represented with a new α_{new}. In order to make this representation, two different approaches were used. In the first one, a trailing edge flap connected at the $0.7c$ point was suggested. With the flap, it was possible to represent the chordline with 2 straight lines and calculate the ΔC_L with flap with thin airfoil theory. In the second method, the whole chordline was modelled as a cambered airfoil and zero-lift angle, α_{L0} was found again with usage of thin airfoil theory [5] and introduced as $\Delta\alpha$, *decamber angle*. These two methods are discussed in the following in a detailed manner.

Modelling with a flap

In Fig.2.11 representation of the modeled chordline at the very tip can be seen. The green line represents the main angle of attack of the actual decambered chordline and the blue line is the attached flap at $0.7c$ point.

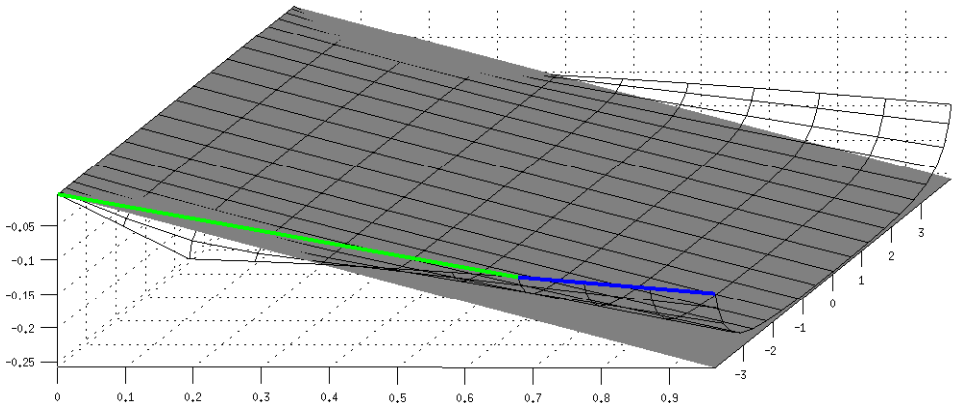

Figure 2.11: Modeling decambered chordline with a flap

In order to calculate the aerodynamic behavior of the modeled flap thin airfoil theory is used [5].

$$\Delta C_L = [2(\pi - \theta_k) + 2sin\theta_k]\delta_f \tag{2.17}$$

In the eq.2.17, δ_f is the flap angle and the θ_k is calculated as;

$$\theta_k = cos^{-1}(1 - 2k) \tag{2.18}$$

where k represents the hinge point for the flap and is 0.7 for this case.

Application of eq.2.17 to all the stations on the wing will give us the ΔC_l for the each spanwise decambered chorline. With an updated C_L data, new circulations can be computed which will re-change the decambering angles. Thus, it can be said that, in order to achieve decambered wing results, iterations (see the Fig.2.6) must be conducted.

Finding a zero lift angle

Although the introduced flap, represents the decambered chordline in an improved way in comparison with a linear line, 3-point-representation is not yet enough for non-linear decambering on a chordline. Moreover, due to subtracted quarter-chord inductions, quality of the 3-point-representation is imperfect close to leading edge as seen from the Fig.2.11). To overcome this issue and to have a fully satisfying, concrete representation of the actual decambered chord, eq.2.19 is used from the thin airfoil theory [5].

$$\alpha_{L0} = -\frac{1}{\pi}\int_0^\pi \frac{d\eta}{dx}(cos\theta - 1)d\theta \tag{2.19}$$

where α_{L0} is the zero lift angle and $\frac{d\eta}{dx}$ is the local slope of the chord. The integration limits in the equation above are from 0 to π which represent the leading and trailing edge, respectively. In order to calculate this integration numerically, some collocation

points were required which are chosen to be cosine distributed 11 chordwise control points. The representation is shown in Fig.2.12.

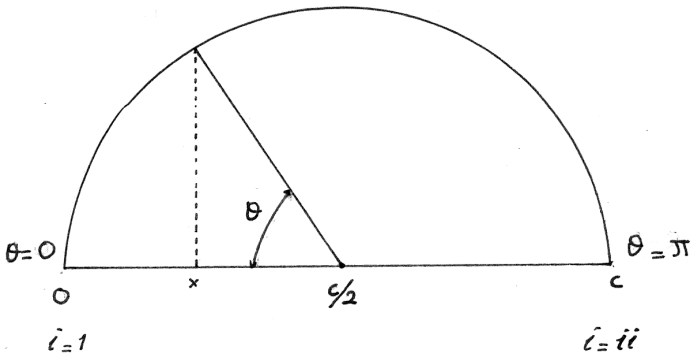

Figure 2.12: Cosine discretization of control points [5]

For every chordwise control point, the total induction $u_{i(i)}^{\rightarrow}$ from the wake needs to be calculated. The i subscript stands for chordwise control point number. Calculation of $u_{i(i)}^{\rightarrow}$ for a 3-bladed wind turbine rotor is shown below;

$$u_{i(i)} = \sum_{B=1}^{B_N} \sum_{J=1}^{N} \sum_{K=1}^{M} u_{i(i,B,J,K)} \tag{2.20}$$

where J stands for number of trailing vortex goes from 1 to total number of spanwise trailing vortices on a single blade, and B is the subscript for blade number from 1 to total number of blades, which is $B_N = 3$ for our case. The K is the subscript for line vortices in a discretized helical vortex convecting through downstream(see the Fig.2.13) with a total number of M. Simply, $u_{i(i,J,B)}$ is the induction calculated from the K^{th} vortex line on the trailing vortex J which is released from the blade number B.

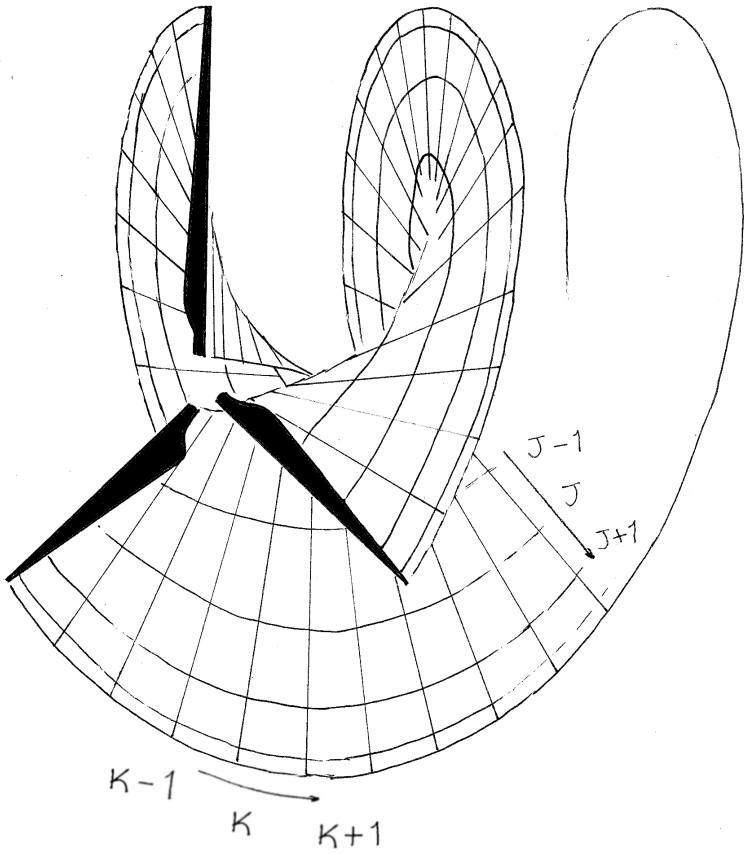

Figure 2.13: Sketch of a 3-bladed wind turbine rotor with discretized helical vortices convecting through downstream

$$\left(\frac{d\eta}{dx}\right)_{(i)} = \frac{\vec{u_{i(i)}} \cdot \vec{n_0}}{\vec{u_{i(i)}} \cdot \vec{n_1} + \vec{u_\infty} \cdot \vec{n_1}} \tag{2.21}$$

The numeric form of eq.2.19 for a selected chordline becomes

$$\alpha_{L0} = -\frac{1}{\pi} \sum_{i=1}^{ii} \left(\frac{d\eta}{dx}\right)_{(i)} (cos\theta_{(i)} - 1)(d\theta)_{(i)} \tag{2.22}$$

where the i subscript represents the chordwise point number to a maximum ii. In this work, it was concluded that 11 points with a cosine distribution on the chordline is enough for modeling decambering. Although this method is computationally more expensive than flap calculation, it was selected for application process due to its satisfactory decambered chordline representation with 11 points.

Chapter 3

Implementation of Decambering Correction

The application of decambering will be handled in this part of the thesis. First, decambering on a planar wing without rotation, and secondly, on a wind turbine rotor will be presented and discussed in detail.

3.1 Non-Rotating Planar Wing

In this section a planar wing with an aspect ratio of 8 will be handled. For circulation calculations, a single panel and a lifting line method with prescribed wakes were used. The wake expansion and roll-up effects were disregarded. The selected airfoil profile for the wing was a NACA0012 which is a zero-camber airfoil and the geometrical angle of attack of the wing was 5 degrees. The reason for a zero-camber-airfoil selection was to be able to compare panel and lifting line results without having an extra unknown effect in circulations since the single panel method is not capable of modeling the camber with only one control point.

Calculating the circulations with respect to C_L data which was $2\pi\alpha$, was straight forward with lifting line iterations. For the correction part, inductions through the control points were found from the known circulation distribution from lifting line results and resulted $\Delta\alpha$ is added to corresponding spanwise station as a correction and new circulations were found. This process is conducted in an iterative manner. For the first iteration, the decambering $\Delta\alpha$ was usually way higher than the converged resulting value and big α change in the first iteration was leading to non-converging, unsteady solutions. In order to avoid this a relaxation factor δ was introduced. The usage is described below.

$$\alpha_{new} = \alpha_{LLT} + \Delta\alpha \tag{3.1}$$

$C_{L(new)}$ is a function of α_{new} which is used directly in $C_L = 2\pi\alpha$. As a result, circulation strength Γ^* from the first iteration becomes a function of variables shown below

$$\Gamma^* = f\big(\alpha_{new}, U_\infty, chord\big) \tag{3.2}$$

and the updated circulation is found by using the introduced relaxation factor

$$\Gamma_{new} = \Gamma_{old} + \delta(\Gamma^* - \Gamma_{old}) \tag{3.3}$$

δ is inversely proportional to circulation strengths and chord length where the decambering effect becomes relatively high. Simply, it is suggested to select small δ values with high angles of attack or low aspect ratio wings. Having said that, values between 0.01 and 0.1 seemed to work fine for the simulations run for this paper.

The panel method, lifting line and decambering correction applied onto lifting line results are shown below.

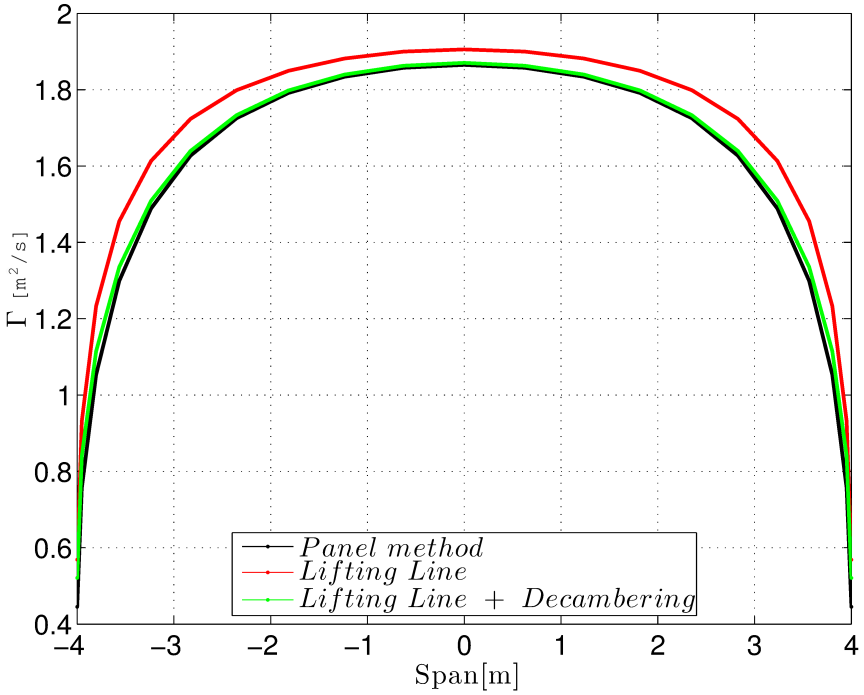

Figure 3.1: Comparison of circulation for a planar wing with LLT, panel method and decambering corrected LLT. AR=8

As seen from the plot, decambering applied lifting line results are very close to the panel method results which was the expectation. Moreover, decambering added lifting line is assumed to have a better representation of circulations in comparison with panel method results since it considers the whole chord instead of a single point at three-quarter chord as panel does. Nevertheless, panel method, without a doubt provides a good information of the magnitude of the effect.

Moreover, at the middle regions, the decambering effects appeart to be still visible. However, with an increased aspect ratio, the influence of the tip vortices decreases and the difference at the middle region, becomes almost none. This change is shown below in Fig.3.2.

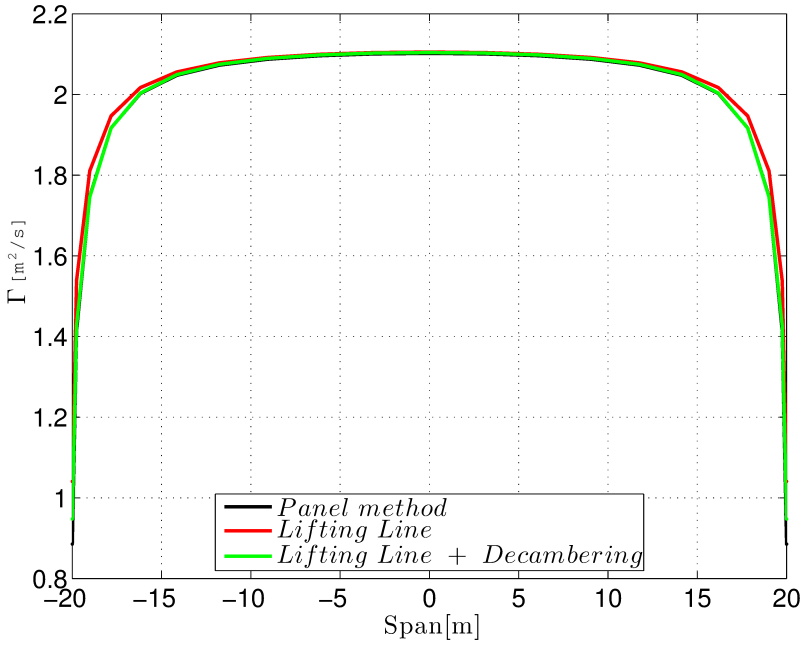

Figure 3.2: Comparison of circulation for a planar wing with LLT, panel method and decambering corrected LLT. AR=40

It can also be said that, with increased aspect ratio, decambering effect decreases due to to raised distance to trailing vortices.

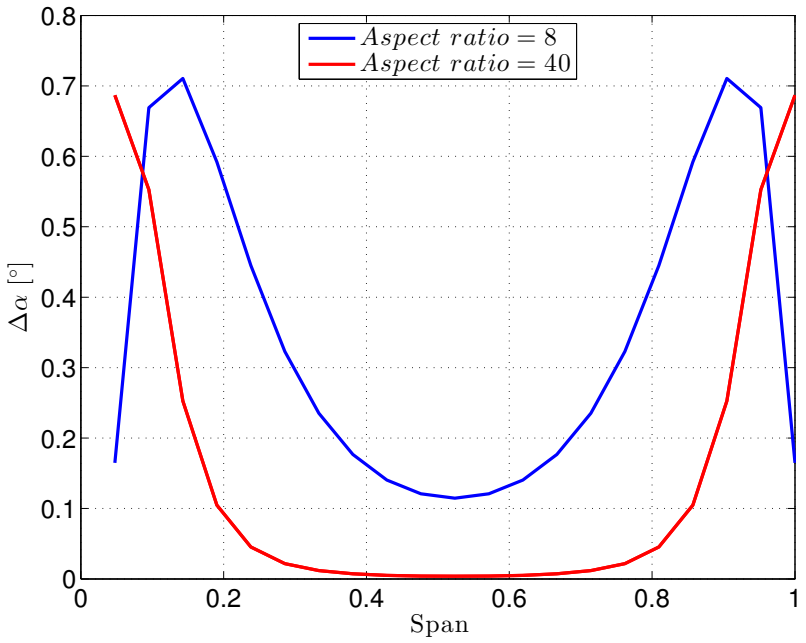

Figure 3.3: Decambering effect in terms of $\Delta\alpha°$, AR=40 versus AR=8

In the Fig.3.3, $\Delta\alpha^\circ$ variety on span caused from the decambering effects are presented for two different types of wings with 8 and 40 aspect ratios. It is clear that increased aspect ratio pushes down the decambering effects for the whole wing as expected.

3.2 Wind Turbine Rotor

In this section, a wind turbine rotor is calculated and decambering correction is applied on the lifting line solution. The wake here used was a prescribed, non-updated wake where the expansion and rolling up effects were disregarded. Thus the trailing vortices were pure helices.

The representation is shown below. Although the figure includes only 3 rotations, the actual calculation is done with 10 rotation wake convection through downstream which corresponds to 3-diameter in terms of axial distance.

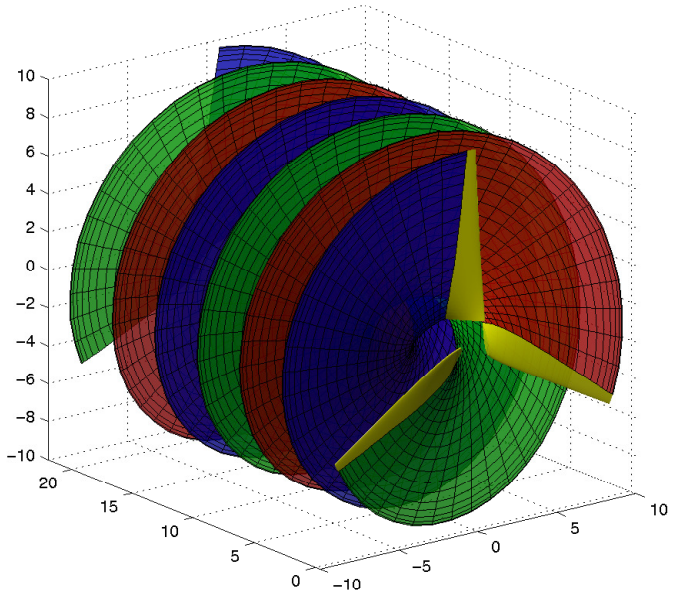

Figure 3.4: Wind turbine rotor and the helical wake geometry

The shedding vortices were also disregarded due to steady inflow. As a result of this, the wake only had trailing vortices discretized with approximately 10 degrees each on each helix.

The blades used for this calculation were designed for $\lambda = 6$ and 5 degrees of design angle of attack with zero-camber NACA0012 airfoil profile. From the root $r = 1$ to tip $r = 10m$, the chord length was linearly varying from 2 to $0.5m$. The twist angles are given below in the table.

Radius $[m]$	1	2	3	4	5	6	7	8	9	10
Twist [°]	44.9	25.9	17.2	12.5	9.5	7.5	6	4.9	4	3.3

With $U_\infty = 8m/s$, and 21 spanwise stations on each blade, the circulations calculated with lifting line, lifting line + correction and panel method are shown below.

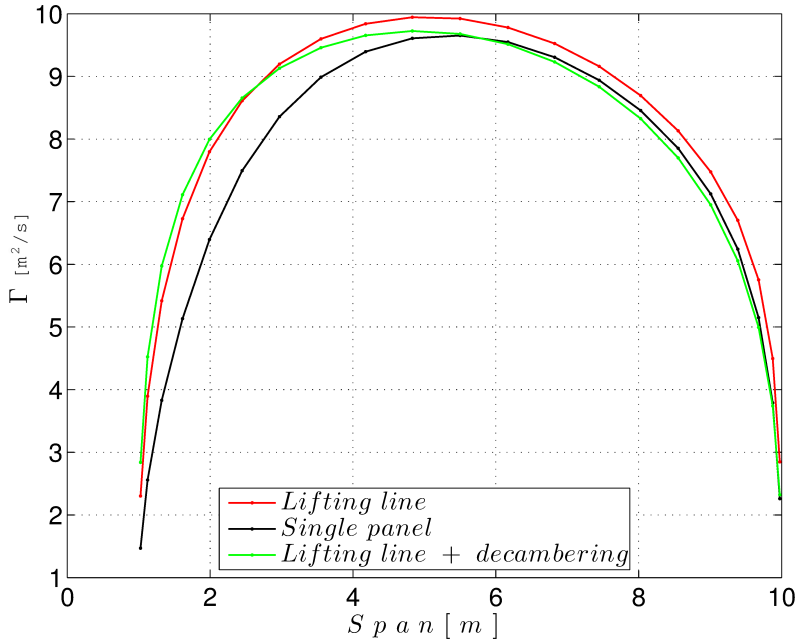

Figure 3.5: Comparison of circulations calculated from different methods

The difference between panel and lifting line can be seen from the Fig.3.5. At outer regions, the correction works as expected and smoothen downs the circulations close to tip, reaches very close to panel results. However, at the root sections, the increase on circulations are seen.

This behavior can be explained with excessive chord lengths close to root which leads an angular change on releasing trailing vortices close to tip regions. Moreover, this is also as a result of having the root section too close to the rotating axis.

During this work, in order to have a satisfying explanation of the increase effect, different blade setups were tried with decambering correction. It was observed that, with rotor blades with shorter chord lengths and outer radius starting positions, the increase weren't occurring.

If we wrap up these application results, for the planar case the decambering correction works very well. On the other hand, regardless of the root increase for long chorded blades, the tip results are also promising for wind turbine rotors. The non-clear root behavior will be re-discussed in the following chapters.

Chapter 4

BEM Application and Validation

In the first part of this chapter, the decambering correction will be applied to the well-known MEXICO rotor and result will be discussed. The validation of the results will be presented in the following section where a new rotor with a cambered airfoil profile will be introduced and comparison results with a full surface panel method will be shown.

4.1 BEM Application

As aforementioned, the correction is based on a vortex method whereas BEM is a 2D model based on the 1D momentum theory. In order to make a coupling with a vortex correction, it was needed to re-introduce a wake with helical vortices.

4.1.1 Generating a Vortex Wake from BEM Solution

In the BEM solution, axial induction factors were found for each spanwise control point which is used for angle of attack calculations. For the correction part these induction factors were used to generate the trailing vortices. To obtain the helical pitch for each released trailing vortex, an axial induction factor from the corresponding spanwise station was used. With respect to the calculated helical pitch, given free stream velocity and rotation speed the helical vortex line was generated. For each spanwise point, local axial induction factor is used as shown below to observe the helical pitch h.

$$h = U_\infty(1 - a_i) \tag{4.1}$$

where a_i is the axial induction factor for corresponding point and U_∞ is the free stream velocity.

4.1.2 Applying the Correction

With defined wake vortices, the correction application was similar to the one for lifting line solution. With the known geometry, the control points were found on the blades surface and inductions from all trailing vortices were calculated and the quarter chord induction is subtracted from inductions that were calculated apriori. With the found

induction change, $\Delta\alpha$ was obtained from thin airfoil theory as explained in Chap.2 and used as an input directly to the BEM as a correction of the corresponding angle of attack without any relaxation factor. The process was conducted in an iterative manner where the wake was also being updated in each iteration step due to changed axial induction factors. The resulting solution with and without correction is shown below for $U_\infty = 5m/s$, $\lambda = 8$ with zero pitch angle.

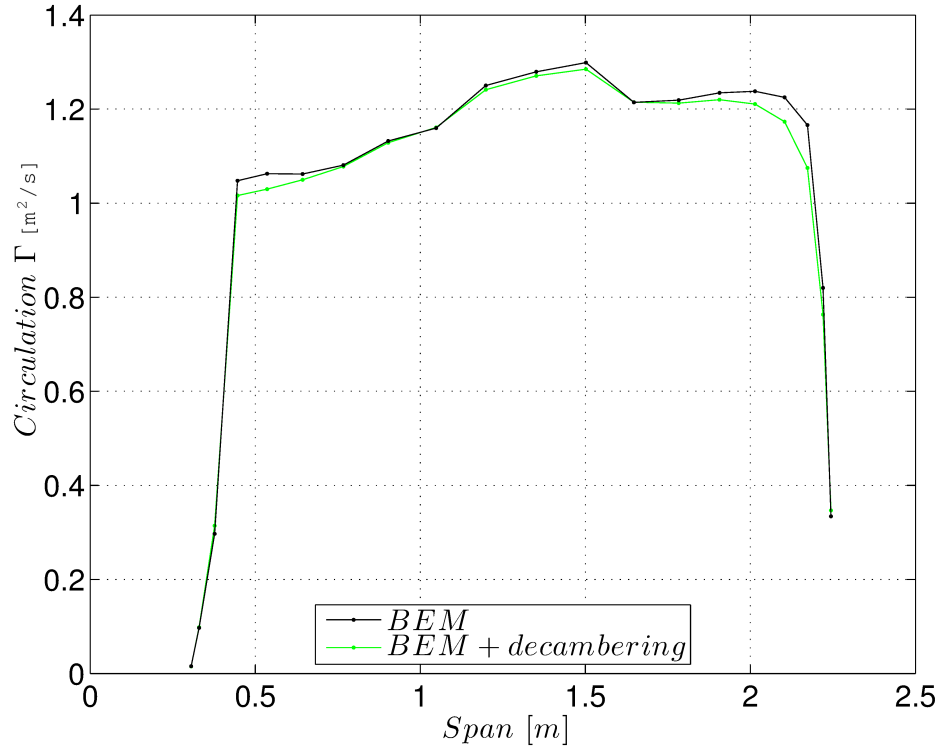

Figure 4.1: Decambering correction applied BEM solution of the Mexico rotor @$U_\infty = 5m/s$

For BEM simulation, the airfoil data is taken from the experimental data (see [3]). From the results, it is clearly seen that the Risø airfoil results with higher C_L values in comparison with NACA and DU cross-sections.

The correction results were generated with 10 rotation downstream wake length with 21 control points. It was observed from different simulations that results with finer spanwise discretizations were resulting the same as 21 points.

As seen from the Fig.4.1, decambering effect trims down the tip circulations. Moreover, at the root region, decreasing effect also visible unlike the lifting line result as shown in the previous chapter. This behavior can be explained by sharper circulation increase at the root region and shorter chord lengths of the blade compared with the one used in lifting line decambering results.

4.1.3 Iterative Approach

The iterative procedure is presented below in Fig.4.2.

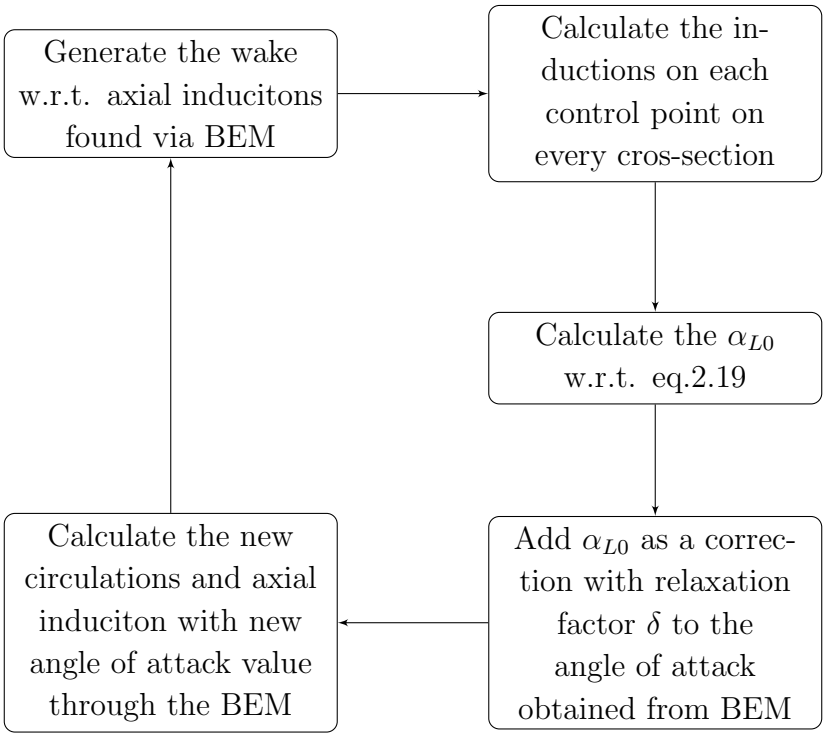

Figure 4.2: Decambering correction iterative procedure

As seen, due to changed circulations and wake geometry, decambering correction needs to be calculated in an iterative manner.

In the Fig.4.1, the presented decambering correction applied circulation distribution is the converged result after 10 cycles with relaxation factor δ of 1 (practically not relaxed). However, when we compare the converged solution with the very first iteration step, we don't see much difference. In the figure below, error comparison is presented based on circulation values resulted at the end of 10^{th} iteration for given conditions.

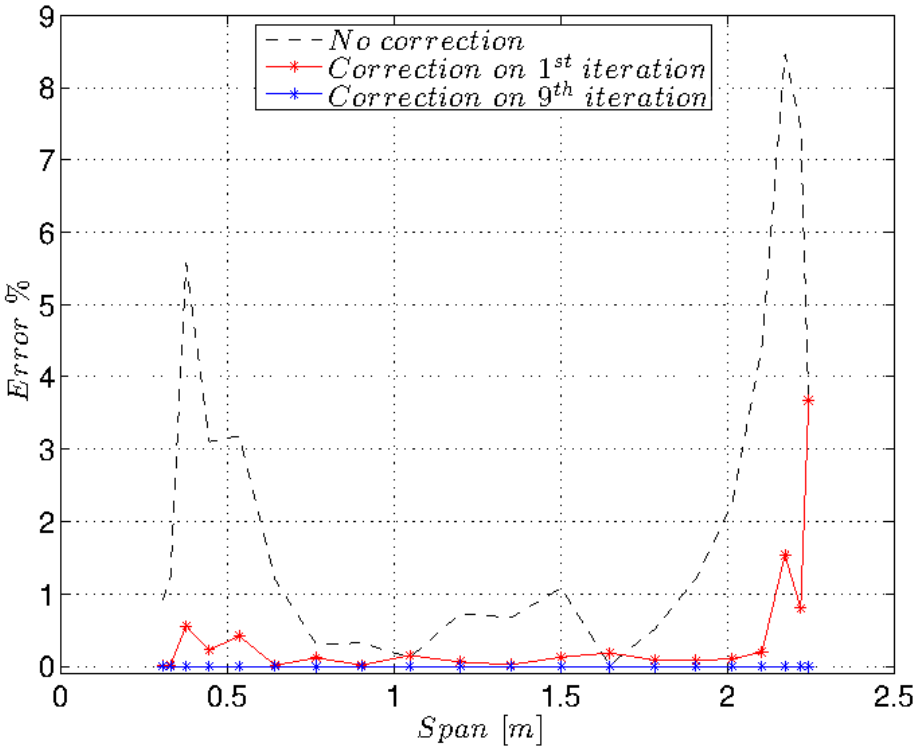

Figure 4.3: Absolute error % of the correction with different iterations

As seen from the Fig.4.3, the maximum absolute error in comparison with converged solution is less than 4% with a single iteration. Furthermore, it can be observed from the 9^{th} iteration that the results were converged already. Although this is not the case for lifting line solutions where the circulation jumps are not as sharp as the BEM results, it can be said for the BEM correction that the single step iteration results are close to the converged results.

It is worthwhile to mention that Montgomerie's comment was quite reasonable which he stated that there would be not much of a change at the tip regions with iterations since there were no changes seen at the middle regions (see the Sect.1.2). In this work, however, it was seen that although middle regions weren't changing with iterations, some changes up to 4% in circulations were noticed after the first iterations at the tip.

In comparison with non-corrected BEM results, decambering correction yields to changes on circulations up to 9% which is directly proportional to the generated lift force as shown before (see the Equ.2.13).

4.2 Validation

In this part a comparison between a full surface panel code and suggested decambering correction method with BEM and lifting line was presented. The surface panel simulations were conducted with the DTU's MIRAS code which is a free wake full surface panel solver with a viscous-inviscid coupling model inside [2]. In this work, only inviscid solutions were used.

For the validation purpose, a new blade was designed with a NACA4412 profile with radius from 0.2 to $1m$ and chord length was varying from 0.156 to $0.06m$ linearly from root to tip. The optimum twist angle β was found by using the equation given below with $\lambda = 6$ [7].

$$\beta = tan^{-1} \frac{2\lambda\left(\frac{r}{R}\right)}{3\lambda^2\left(\frac{r}{R}\right)^2 + 2} \tag{4.2}$$

For the lifting line calculation a free wake method was used where the wake vortices were convected downstream with respect to the inductions and free stream velocity. The length of the wake was as equal as 8 rotation, downstream convected wake length. In the calculation, a uniform $U_\infty = 8m/s$ was given. For all of the simulation cases, flow assumed to be inviscid and C_L coefficients were taken from Xfoil for lifting line and BEM. Moreover, it is good to mention that for the lifting line case, decambering was applied as a step forward when the simulation was finished. The correction could also be applied during the time stepping while the wake was forming. The comparison results are shown below.

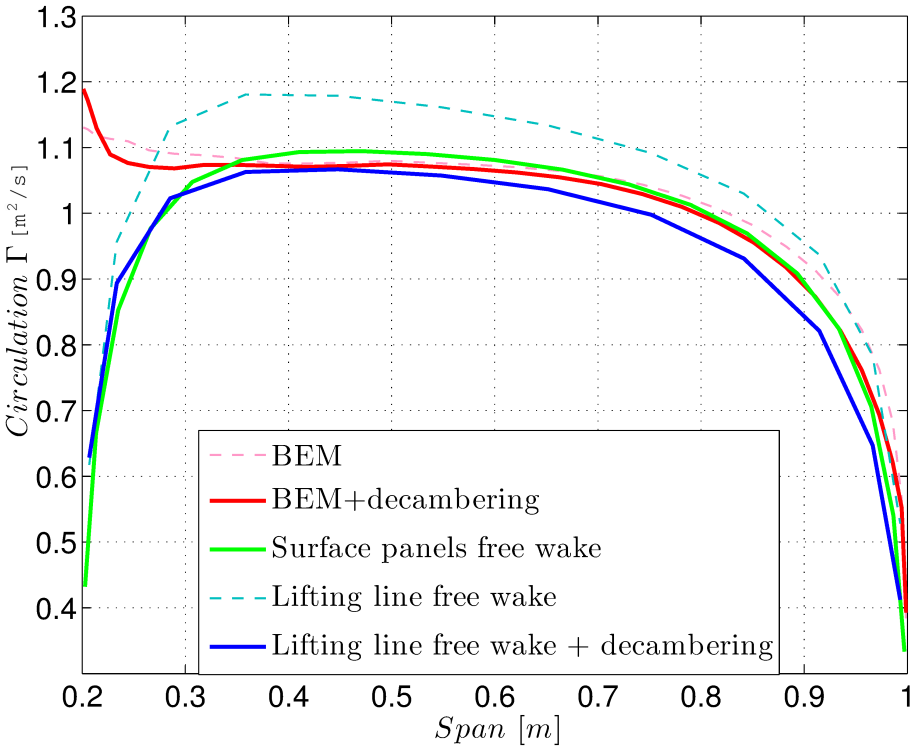

Figure 4.4: Comparisons with different models

The surface panel method considered as the most realistic approach and taken as a base line for comparisons. As seen, the free wake lifting line simulation resulted with relatively high circulations as expected due to not-included decambering effects. With the correction, a high drop in lifting line circulations was observed and resulting values were lower than surface panel results.

The BEM results, at the root regions, were rather high in comparison with others which can be explained by not-included tip effects and harsh start with a large airfoil cros-section. Since the solver is based on 2D, it is not capable of modeling the leakage effects at the root section and resulted with the highest circulations at the root. On the other side, the tip region, this is being handled with the tip corrections. It can be said that with applied decambering correction, tip circulations became very close to the surface panel results which was more than satisfying.

Chapter 5

Conclusions and Future Work

Throughout this thesis, a decambering correction method was developed and applied as an add-on to the BEM results with tip correction. As was expected, the decambering effect caused lift drops mainly at the tip regions and calculations showed that the applied correction was pulling down the circulations to the values found by surface panel methods which was considered as the most real. Especially, considering the simplicity and rapidity of the BEM method, the correction can be considered as a good step forward for 2D based calculations.

On the other hand, the decambering corrected lifting line results were also satisfying. The occurred discrepancy in circulations can be explained with the coarse time stepping in free wake code and coarse discretization of control points on the blade due to excessive calculation times. The free wake lifting line code was coded in Matlab and run with 12 shared memory cores in parallel where each control point was handled with a single core. However, 12 control points were not enough for dissolving the blade and a single time step was corresponding to 20° of revolution which was considered as rough. Furthermore, as aforementioned, the decambering correction was applied as an add-on to the free wake lifting line solutions with the found geometry of the wake. Nevertheless, it can be said that the wake geometry would be in a different form if the correction was being used in each time step instead where the wake was forming. Although this was known, it wasn't possible to apply decambering inside the time steps due to slow calculations as a result of using Matlab as a coding language.

Future Work

First of all, it seemed from the results that the suggested model was good at predicting decambering effects with either BEM or lifting line. However, for applications it needs to be validated with more simulations. As a next step, it is suggested to have a comparison between a full surface panel method and a free wake lifting line on a non-rotating planar wing. Both simulations should have the exact same vortex core models and the lifting line method should have the correction model in each time step with sufficient number of control points on the wing. Such comparisons with different aspect ratios would provide reliable information before the usage.

The results presented in this paper were generated with 10 wake revolutions for decambering induction calculations where the computational cost was quite high. During the

work, it was observed that a half revolution of the wake is already sufficient to calculate the decambering effect for the BEM application. With this information, it is suggested that, a single-revolution-wake decambering correction can also be applied instead which will decrease the computing cost.

In further steps, the method can be put into a black box 3D correction software. Simply, the ingredients for the correction are the resulting circulations, which can be obtained from BEM simulations, chord lengths and the distances to the root for each spanwise station or in simple terms: the geometry of the blade.

References

[1] Emmanuel Branlard. Wind turbine tip-loss corrections. Master's thesis, The Technical University of Denmark, 2011.

[2] N. R. García, J. Sørensen, and W.Z. Shen. Three-dimensional viscous-inviscid cupling method for wind turbine computations. Research article, Wind Energy.

[3] J. G. Schepers K. Boorsma. Description of experimental setup, mexico measurements. ECN.

[4] C. Gundling K. Brown and J. Sitaraman. Fast multipole accelerated free-vortex simulations of the lillgrund wind farm. Technical report, University of Wyoming, Department of Mechanical Engineering, 2013.

[5] J. Katz and A. Plotkin. *Low-Speed Aerodynamics, 2nd Edition*. Cambridge University Press, 2001.

[6] B. Montgomerie. Explanation of an effect of lift reduction near the tip caused by the local flow around airplane wings or wind turbine tips. Technical report, ECN, April 1995.

[7] David Sharpe Tony Burton, Nick Jenkins and Ervin Bossanyi. *Wind Energy Handbook*. John Wiley & Sons Ltd., 2011.

[8] O. Uzol and N. S. Uzol. Free-wake calculations of wind turbine wake-rotor interactions. Making Torque Conference, Oldenburg, Germany, October 2012.

[9] A. van Garrel. Development of a wind turbine aerodynamics simulation module. Technical report, ECN, 2003.

DTU Vindenergi er et institut under Danmarks Tekniske Universitet med en unik integration af forskning, uddannelse, innovation og offentlige/private konsulentopgaver inden for vindenergi. Vores aktiviteter bidrager til nye muligheder og teknologier inden for udnyttelse af vindenergi, både globalt og nationalt. Forskningen har fokus på specifikke tekniske og videnskabelige områder, der er centrale for udvikling, innovation og brug af vindenergi, og som danner grundlaget for højt kvalificerede uddannelser på universitetet.

Vi har mere end 230 ansatte og heraf er ca. 60 ph.d. studerende. Forskningen tager udgangspunkt i 9 forskningsprogrammer, der er organiseret i tre hovedgrupper: vindenergisystemer, vindmølleteknologi og grundlag for vindenergi.

Danmarks Tekniske Universitet
DTU Vindenergi
Nils Koppels Allé
Bygning 403
2800 Kgs. Lyngby
Telefon 45 25 25 25
info@vindenergi.dtu.dk
www.vindenergi.dtu.dk